of our results, it is reasonable to expect that our findings may generalize to other mid-latitude marine pelagic ecosystems. Under such a scenario, impacts will undoubtedly be felt not only in the oceans, but also in terrestrial ecosystems globally.

### References and Notes


1. P. G. Falkowski, R. T. Barber, V. Smetacek, *Science* **281**, 200 (1998).
2. D. Roemmich, J. McGowan, *Science* **267**, 1324 (1995).
3. L. Hughes, *Trends Ecol. Evol.* **15**, 56 (2000).
4. G. Beaugrand, P. C. Reid, F. Ibañez, J. A. Lindley, M. Edwards, *Science* **296**, 1692 (2002).
5. P. Cury *et al.*, *ICES J. Mar. Sci.* **57**, 603 (2000).
6. N. J. Aebischer, J. C. Coulson, J. M. Colebrook, *Nature* **347**, 753 (1990).
7. X. Irigoien, J. Huisman, R. P. Harris, *Nature* **429**, 863 (2004).
8. G. M. Daskalov, *Mar. Ecol. Prog. Ser.* **225**, 53 (2002).
9. F. Micheli, *Science* 285, **1396** (1999).
10. J. B. Shurin *et al.*, *Ecol. Lett.* **5**, 785 (2002).
11. P. C. Reid, J. M. Colebrook, J. B. L. Matthews, J. Aiken, *Prog. Oceanogr.* **58**, 117 (2003).
12. G. Beaugrand, K. M. Brander, J. A. Lindley, S. Souissi, P. C. Reid, *Nature* **426**, 661 (2003).
13. B. Worm, R. A. Myers, *Ecology* **84**, 162 (2003).
14. The spatial, temporal, taxonomic, and ecological scales considered here force some simplifications. For example, all abundance estimates in this study represent indices of near-surface plankton abundance and not absolute values, because the CPR is towed at a depth of ~10 m and many taxa, especially smaller ones, are caught only semiquantitatively. We calculate abundance rather than biomass time series for each trophic level because neither mass nor length measurements are taken from CPR samples, so biomass estimates would require additional assumptions. Within the coarse trophic categories in this study, members (supporting online text) are deemed to be generalist feeders, so each is considered a functional group. Although the phytoplankton compartment does not include nanoflagellates (they are too delicate to be preserved on CPR silks), we are primarily interested in phytoplankton as food for herbivorous copepods, and these feed preferentially on the larger phytoplankton. The zooplankton carnivore compartment includes data on siphonophore abundance, but corresponding data for other cnidarians are not available due to damage during sampling. We do not include meroplankton because their dynamics can be heavily influenced by processes independent of the pelagic ecosystem. We also do not include various other functional groups such as picoplankton, fish, birds, or marine mammals because time series are not available at the appropriate scales for our study. Thus, our conclusions can only be applied to groups sampled quantitatively by the CPR and cannot easily be extended to include the entire pelagic ecosystem.
15. H. A. Bouman *et al.*, *Mar. Ecol. Prog. Ser.* **258**, 19 (2003).
16. We do not use wind or hydrographic (current) data because they have differential effects over the study domain. Reliable time series for clouds are rare over the entire study period (1958 to 2002) and domain. We also do not use an integrative environmental index such as the NAO because it does not allow analysis of the direct responses of plankton communities to their local environment, and because the effects of climate change on the NAO are less clearly understood than are those on SST.
17. J. M. Colebrook, *Bull. Mar. Ecol.* **8**, 143 (1975).
18. B. J. Pyper, R. M. Peterman, *Can. J. Fish. Aquat. Sci.* **55**, 2127 (1998).
19. To apply the modified Chelton Method we estimated autocorrelation functions for each time series. Because many were broken, we used a spline smoother to interpolate data for up to two missing years. These interpolated data were used only to determine the number of degrees of freedom to be removed from analyses; in no way were they used to inflate the time series or to alter correlation coefficients.
20. B. Planque, T. Frédou, *Can. J. Fish. Aquat. Sci.* **56**, 2069 (1999).
21. W. K. W. Li, *Nature* **419**, 154 (2002).
22. K. L. Carder, F. R. Chen, Z. P. Lee, S. K. Hawes, D. Kamykowski, *J. Geophys. Res.* **104**, 5403 (1999).
23. S. Sathyendranath, G. Cota, V. Stuart, H. Maass, T. Platt, *Int. J. Remote Sens.* **22**, 249 (2001).
24. J.-M. Fromentin, B. Planque, *Mar. Ecol. Prog. Ser.* **134**, 111 (1996).
25. J. W. Hurrell, *Science* **269**, 676 (1995).
26. D. H. Cushing, *J. Plankton Res.* **11**, 1 (1989).
27. C. M. O'Brien, C. J. Fox, B. Planque, J. Casey, *Nature* **404**, 142 (2000).
28. L. S. Parsons, W. H. Lear, *Prog. Oceanogr.* **49**, 167 (1999).
29. J. T. Houghton *et al.*, Eds., *Climate Change 2001: The Scientific Basis* (Cambridge Univ. Press, Cambridge, 2001).


30. We thank A. Lindley and M. Gibbons for helping us assign zooplankton to functional groups, as well as the Hadley Centre, UK Met Office, for providing the SST data (HadISST Version 1.1) at no cost. D.S.S. gratefully acknowledges the funding generously provided for this work by the South African National Research Foundation (GUN 2053579), the Ernest Oppenheimer Memorial Trust, and the University of Port Elizabeth, and A.J.R. acknowledges the financial support of Department of Environment Food and Rural Affairs contract MFO430. The CPR survey would not be possible without the cooperation of the agents, owners, masters, and crews of the vessels that tow the recorders. A funding consortium made up of governmental agencies from Canada, France, Iceland, Ireland, the Netherlands, Portugal, the United Kingdom, and the United States financially supports the survey. CPR data are available freely to the international scientific community for research (see www.sahfos.org).


**Supporting Online Material**

www.sciencemag.org/cgi/content/full/305/5690/1609/DC1
SOM Text
Table S1
References

1 June 2004; accepted 10 August 2004

# Methanobactin, a Copper-Acquisition Compound from Methane-Oxidizing Bacteria

**Hyung J. Kim,[1]* David W. Graham,[1]† Alan A. DiSpirito,[5] Michail A. Alterman,[2] Nadezhda Galeva,[3] Cynthia K. Larive,[4] Dan Asunskis,[6] Peter M. A. Sherwood[6]**

**Siderophores are extracellular iron-binding compounds that mediate iron transport into many cells. We present evidence of analogous molecules for copper transport from methane-oxidizing bacteria, represented here by a small fluorescent chromopeptide ($C_{45}N_{12}O_{14}H_{62}Cu$, 1216 daltons) produced by *Methylosinus trichosporium* OB3b. The crystal structure of this compound, methanobactin, was resolved to 1.15 angstroms. It is composed of a tetrapeptide, a tripeptide, and several unusual moieties, including two 4-thionyl-5-hydroxyimidazole chromophores that coordinate the copper, a pyrrolidine that confers a bend in the overall chain, and an amino-terminal isopropylester group. The copper coordination environment includes a dual nitrogen- and sulfur-donating system derived from the thionyl imidazolate moieties. Structural elucidation of this molecule has broad implications in terms of organo-copper chemistry, biological methane oxidation, and global carbon cycling.**

The mechanisms involved in microbial copper homeostasis are rapidly being elucidated, although the workings of such systems are only understood in model organisms such as *Escherichia coli*, *Enterococcus hirae*, and *Saccharomyces cerevisiae* (*1–4*). In these organisms, copper homeostatic systems are geared toward active detoxification as opposed to accumulation and storage. However, in many methanotrophic bacteria (aerobes that oxidize $CH_4$ for carbon and energy and play a major role in the global carbon cycle), copper homeostasis differs because copper requirements can be up to fourfold higher than iron requirements (*5–7*). In such methanotrophs, copper plays a central role in metabolism, regulating expression of two methane monooxygenases: a soluble methane monooxygenase (sMMO) and particulate methane monooxygenase (pMMO) (*5*, *8–10*). Copper also influences the expression of at least two of the four formaldehyde dehydrogenases (*11–13*), the development of internal membranes (*5*, *8*, *14*, *15*), and the expression of other polypeptides related to copper regulation or transport (*5*, *16–19*).

Given the notable role of copper in methanotroph physiology, we postulated that these

[1]Department of Civil, Environmental, and Architectural Engineering, [2]Biochemical Research Service Laboratory, [3]Mass Spectrometry Laboratory, [4]Department of Chemistry, University of Kansas, Lawrence, KS 66045, USA. [5]Department of Biochemistry, Biophysics, and Molecular Biology, Iowa State University, Ames, IA 50011, USA. [6]Department of Chemistry, Kansas State University, Manhattan, KS 66506, USA.

*Present address: Department of Biochemistry, Molecular Biology, and Biophysics, University of Minnesota, St. Paul, MN 55108, USA.
†To whom correspondence should be addressed. E-mail: dwgraham@ku.edu

organisms possess a specialized copper-trafficking mechanism dedicated to transporting higher amounts of copper while protecting cellular components from its toxic effects. Several low–molecular weight copper-containing compounds, previously called copper-binding compounds (CBCs), were implicated in such a mechanism (*5*, *7*, *20–22*); however, sizes among CBCs varied, and no complete structures could be determined. We now suspect that many of the compounds identified earlier were actually breakdown products of a primary molecule described here, which we identify as methanobactin.

Methanobactin appears to fulfill all the presumed roles of such a copper-trafficking molecule. Methanobactin accumulates to high amounts in the growth media of *Methylosinus trichosporium* OB3b and *Methylococcus capsulatus* Bath when grown under copper-limited conditions; however, it is rapidly internalized into the cell when copper is provided. Furthermore, methanobactin stimulates growth in copper-grown *M. trichosporium* OB3b with an optimal 1:1 copper:methanobactin binding stoichiometry (*23*), and copper uptake–deficient mutants accumulate methanobactin in their growth medium in the presence of copper (*20–22*). Lastly, methanobactin co-purifies with pMMO at ratios of 8 to 13 methanobactins per pMMO complex, and the removal of methanobactin results in the loss of pMMO activity in cell-free systems (*5*, *7*). These combined results suggest a previously unknown copper acquisition system in *M. trichosporium* OB3b, mediated by a molecule or molecules that resemble iron siderophores in other bacteria. Furthermore, given the limited understanding of the molecular structure of pMMO and the mechanism of methane oxidation by this enzyme, investigations into the structure and function of methanobactin are of interest.

Here, we report the complete crystal structure of methanobactin excreted into the growth media by *M. trichosporium* OB3b. Typically, 15 to 20 mg of this yellowish-red compound is isolated per liter of spent medium with 3-day-old copper-limited cultures [optical density at 600 nm ($OD_{600nm}$) ~ 0.7], but the yield is heavily dependent on extracellular copper amounts, copper-to-biomass ratios, and culture ages. Purification of the compound involved solid-phase extraction and reversed-phase high-performance liquid chromatography (RP-HPLC) (*23–25*). Mass spectrometry (MS) of the isolated product showed two predominant ions differing in mass by 62 daltons (Fig. 1). The peak with $[M - H]^-$ at *m/z* 1153 was assigned to the molecular ion for the deprotonated compound, whereas the most intense peak at *m/z* 1215 was assigned to the corresponding copper complex $[M - 2H + {}^{63}Cu^+]^-$. Additionally, this signal shows an isotopic distribution characteristic of copper (69.2% $^{63}Cu$, 0% $^{64}Cu$, and 30.8% $^{65}Cu$).

X-ray photoelectron spectroscopy (XPS) analysis (*25*, *26*) of the methanobactin-copper complex indicates that the majority of the copper is present as $Cu^+$. Some $Cu^{2+}$ is noted after extended exposure to air, but this is atypical of physiological conditions and the predominant copper oxidation state in methanobactin is $Cu^+$ (*24*). Figure 2 presents the XPS binding energy spectra for the copper 2p region for freshly bound copper-methanobactin and CuO, which indicate two low-intensity satellite features (peaks 2 and 3) and a shifted position of the main peaks (1 and 4) relative to CuO, characteristic of $Cu^+$. This observation is consistent with an earlier electron paramagnetic resonance study (*7*) and is similar to other cell systems with mediated copper transport (*27*).

The overall structural features of methanobactin, including amino acid composition and sequence, and N- and C-terminus identification were established by a combination of biochemical and mass spectroscopic analyses (*23–25*). The presence of unusual residues was deduced from a significant mass difference (> 358 daltons) between sequence data and MS investigations. Early results suggested that methanobactin was composed of about 10 to 12 residues arranged in a nonlinear motif with a high affinity for copper. Methanobactin was subsequently crystallized (*23*, *25*), and the structure was resolved by direct methods and refined by full-matrix least-squares methods on $F^2$ to 1.15 Å (*28*).

Crystallographic data (Table 1) indicate that methanobactin is a small chromopeptide that contains one copper ion per molecule, coordinated by a previously unobserved ligand system with a peptide backbone comprising amino acid and non–amino acid residues. The primary sequence of methanobactin is *N*-2-isopropylester–(4-thionyl-5-hydroxy-imidazole)–$Gly^1$–$Ser^2$–$Cys^3$–$Tyr^4$–pyrrolidine–(4-hydroxy-5-thionyl-imidazole)–$Ser^5$–$Cys^6$–$Met^7$, with an empirical formula of $C_{45}N_{12}O_{14}H_{62}Cu$ (Fig. 3A). Methanobactin is observed as a crystallographic dimer (fig. S1), although the apparent lack of direct interactions

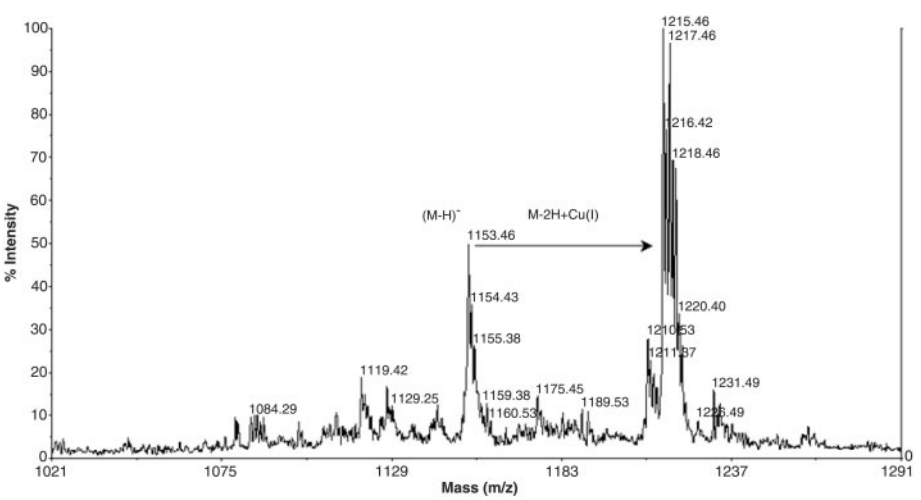


**Fig. 1.** Negative-ion MALDI-TOF mass spectrum of extracellular copper compound from *M. trichosporium* OB3b showing copper complexation. The isotopic distribution of the most dominant peak is that of copper.

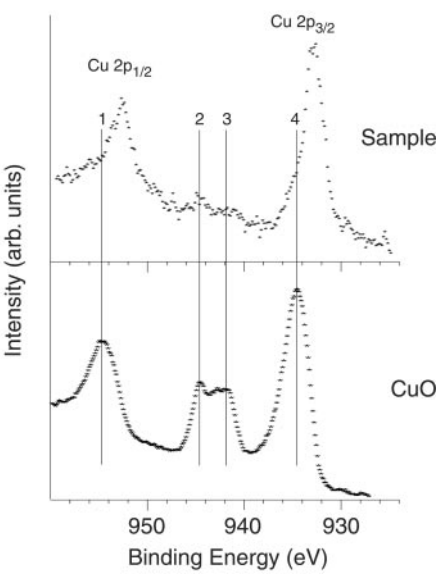


**Fig. 2.** XPS binding energy spectra for the copper 2p region for methanobactin and for CuO, a reference compound that has copper in the formal oxidation state of $Cu^{2+}$. The low intensity of the satellite features (2 and 3) and the shifted position of the Cu $2p_{1/2}$ and Cu $2p_{3/2}$ peaks (1 and 4) in methanobactin indicate that copper is primarily in the $Cu^+$ oxidation state.

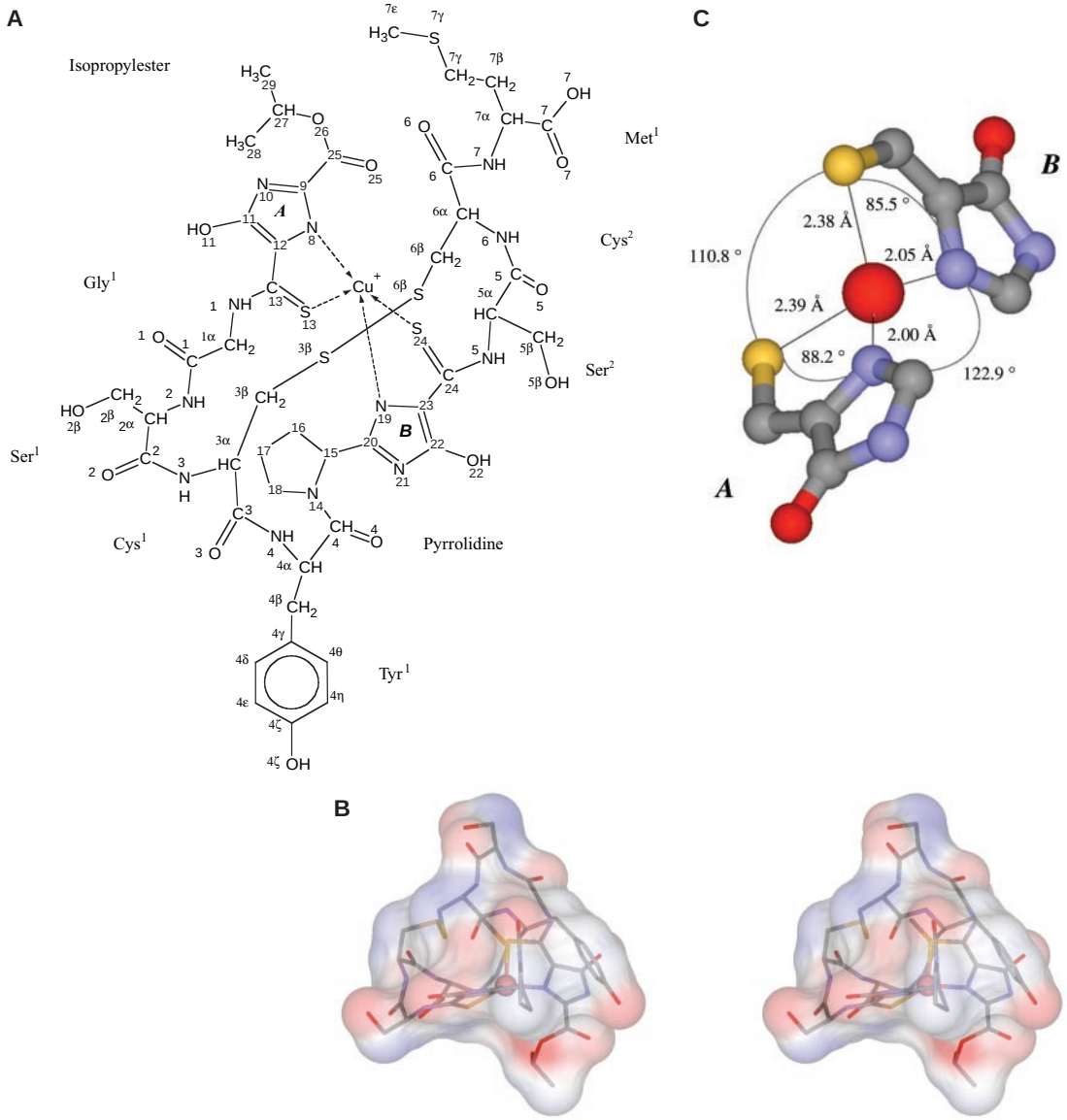


**Fig. 3.** (**A**) Schematic drawing of methanobactin along with the International Union of Pure and Applied Chemistry atom numbering scheme used in the text. (**B**) The copper coordination sphere derived from 4-hydroxy-5-thionyl imidazoles. Atom colors: carbon, gray; oxygen, red; nitrogen, blue; and sulfur, yellow. Copper ion is represented by central red sphere. (**C**) Stereoview of methanobactin surface modeled with the use of solvent-molecule interaction (probe interaction is 1.4 Å).

between each component suggests that the dimerization in crystals does not persist in solution and is not physiologically relevant.

Overall, methanobactin can be described as having a very compact pyramid-like shape (Fig. 3B) with the metal complexation site being located at the base of the pyramid and not buried. The isopropylester group folds underneath this surface, creating a tail-like projection and a cleft, and appears to obscure the metal site to some extent. The metal coordination environment is composed of dual N- and S-donating systems that are derived from two 4-thionyl-5-hydroxy imidazolate moieties. The bond distances between the donating sulfur atom and its adjacent carbon are 1.68 Å (in thionyl imidazolate A) and 1.67 Å (in thionyl imidazolate B) (Fig. 3C). The sulfur is thus modeled as a thionyl ligand (C=S–Cu) rather than the more commonly found thiolate (C–S–Cu). The C=S distances agree well with previous synthetic N,S-thionyl donor complexes that possess antibacterial properties (*29*). Furthermore, the thioamide bonds that link each imidazole moiety to a $Gly^1$ and a $Ser^2$ are found in the thiopeptide antibiotics promoinducin and thiostreptone from the *Streptomyces* species, which is interesting given that methanobactin has also shown to be bacteriocidal for a variety of Gram-positive bacteria (*30*). This unusual thiopeptide bond is also found in the nickel enzyme methyl–coenzyme reductase from methanogenic archaea that catalyzes methane formation from methyl–coenzyme M and coenzyme B (*31*, *32*).

The $N^{\varepsilon}$ atom of each imidazole and the S atom of the two thionyl substituents coordinate the copper in a distorted tetrahedron geometry (Fig. 3C). A solvent molecule is not coordinated to the copper in the crystal structure. The $N^{\varepsilon}(8)$-Cu-S(13) and $N^{\varepsilon}(19)$-Cu-S(24) bond angles (ligand bite angles) of 85.5° and 88.2°, respectively, deviate from the ideal tetrahedral bond angle (109.5°). Both heterocycle rings along with the thionyl substituents are essentially co-planar. The copper atom lies in the plane of thionyl imidazole B but deviates by 0.87 Å from the plane of thionyl imidazole A. The two planes defining the N,S-chromophoric moieties bisect at nearly perpendicular angles. The copper-to-ligand distances are 2.39 and 2.38 Å for Cu-S(13) and Cu-S(24), respectively, and 2.01 and 2.05 Å for $N^{\varepsilon}(8)$-Cu and $N^{\varepsilon}(19)$-Cu (numbers in parentheses designate relative atom numbers), respectively, and indicate strong interactions (Fig. 3C).

The structure of methanobactin as well as growth and physiological data argues for its function as a copper-sequestration compound (*20*–*22*). The cells appear to excrete methanobactin continuously, and it accumulates in the culture media under copper-deficient conditions. If copper is provided, methanobactin binds the copper and the methanobactin-copper

**Table 1.** Crystallographic data and refinement statistics. A total of 1663 parameters were refined against 698 restraints and 8765 data to give wR($F^2$) = 0.2464 and $S$ = 1.1 (where $S$ is goodness of fit) for weights of $w = 1/[\sigma^2(F^2) + (0.1600P)^2 + 130.00P]$, where $P = ([F^2_{obs} - F^2_{cal}])/3$. The final $R$ factor, R($F$), was 0.0824 for the 7025 observed, [$F > 4\sigma$ ($F$)], data. The largest shift/standard uncertainty was 0.012 in the final refinement cycle. The final difference map had maxima and minima of 0.624 and −0.393 e/Å$^3$, respectively. Parentheses denote the highest resolution shell. $R_{sym} = \Sigma[\Sigma|F^2_{obs} - F^2_{cal}|]/\Sigma(\Sigma F^2_{obs})/n]$ and $R$ factor $= \Sigma||F_{obs}| - |F_{cal}||/\Sigma|F_{obs}|$, $F_{obs} > 0$.

| $(C_{44}H_{54}CuN_{12}O_{15}S_5) \cdot 10.5(H_2O)$ | |
|---|---|
| Formula weight | 1404 |
| Molecular weight $(C_{44}H_{54}CuN_{12}O_{15}S_5)$ | 1217.2 |
| *Data collection* | |
| Wavelength | 0.71073 Å |
| Reflections collected | 66,370 |
| *Refinement* | |
| Redundancy | 7.55 |
| I/σ | 18.23 (14.81) |
| Rsym (%) | 8.05 (37.62) |
| Resolution (Å) | 1.15 |
| $R$ factor | 0.0832 |
| Completeness | 99.8 |
| Goodness of fit on $F^2$ | 1.1 |

complex is internalized to the cell, possibly to be associated with pMMO (*5*, *7*, *24*). Further, its metal-ion shuttling role is suggested by structural similarities to the amino acid–containing pyoverdin class of iron siderophores, which also have antibacterial properties (*33*–*36*). In fact, the similarities between methanobactin and the pyoverdin siderophores (e.g., azotobactin and pseudobactin produced by *Azotobacter* spp. and *Pseudomonas* spp.) led to the renaming of CBC to methanobactin.

If methanobactin is indeed a "copper-siderophore" or a "chalkophore" (after the Greek for copper), a specialized copper-trafficking or defense mechanism probably exists in organisms that produce the compound. However, whether methanobactin acts exclusively as an extracellular copper-sequestering agent or has other in vivo functions related to the delivery and insertion of copper ions to copper-containing proteins like pMMO must still be determined. Regardless, the elucidation of the methanobactin structure has major implications in understanding the molecular mechanism of biological methane oxidation and methane cycling in the environment and may also lead to the identification of other copper-trafficking molecules.

**References and Notes**


1. D. L. Huffman, T. V. O'Halloran, *Annu. Rev. Biochem.* **70**, 677 (2001).
2. L. A. Finney, T. V. O'Halloran, *Science* **300**, 931 (2003).
3. C. Rensing, G. Grass, *FEMS Microbiol. Rev.* **27**, 197 (2003).
4. A. C. Rosenzweig, *Chem. Biol.* **9**, 673 (2002).
5. D. W. Choi *et al.*, *J. Bacteriol.* **185**, 5755 (2003).
6. H.-N. Nguyen *et al.*, *J. Biol. Chem.* **269**, 14995 (1994).
7. J. A. Zahn, A. A. DiSpirito, *J. Bacteriol.* **178**, 1018 (1996).
8. H. Dalton, S. D. Prior, D. J. Leak, S. H. Stanley, in *Microbial Growth on $C_1$ Compounds*, R. L. C. Hanson, R. S. Hanson, Eds. (American Society for Microbiology, Washington, DC, 1984), pp. 75–82.
9. S. D. Prior, H. Dalton, *J. Gen. Microbiol.* **131**, 155 (1985).
10. S. Lontoh, J. D. Semrau, *Appl. Environ. Microbiol.* **64**, 1106 (1998).
11. J. A. Zahn, D. J. Bergmann, J. M. Boyd, R. C. Kuitz, A. A. DiSpirito, *J. Bacteriol.* **183**, 6832 (2001).
12. S. Tate, H. Dalton, *Microbiology* **145**, 159 (1999).
13. J. A. Vorholt, L. Chistoserdova, S. M. Stolyar, R. K. Thauer, M. E. Lidstrom, *J. Bacteriol.* **181**, 5750 (1999).
14. C. A. Brantner *et al.*, *Can. J. Microbiol.* **43**, 672 (1997).
15. P. Peltola, P. Priha, S. Laakso, *Arch. Microbiol.* **159**, 521 (1993).
16. O. Berson, M. E. Lidstrom, *Environ. Sci. Technol.* **30**, 802 (1998).
17. H. J. Kim, D. W. Graham, *FEMS Microbiol. Lett.* **201**, 133 (2001).
18. G. P. Stafford, J. Scanlan, I. R. McDonald, J. C. Murrell, *Microbiology* **149**, 1771 (2003).
19. O. A. Karlsen *et al.*, *Appl. Environ. Microbiol.* **69**, 2386 (2003).
20. A. A. DiSpirito *et al.*, *J. Bacteriol.* **180**, 3606 (1998).
21. M. W. Fitch *et al.*, *Appl. Environ. Microbiol.* **59**, 2771 (1993).
22. C. M. Tellez, K. P. Gaus, D. W. Graham, R. G. Arnold, R. Z. Guzman, *Appl. Environ. Microbiol.* **64**, 1115 (1998).
23. H. J. Kim, thesis, University of Kansas (2003).
24. H. J. Kim *et al.*, in preparation.
25. Materials and methods are available as supporting material on *Science* Online.
26. G. D. Claycomb, P. M. A. Sherwood, *J. Vac. Sci. Technol. A* **20**, 1230 (2002).
27. S. Puig, E. M. Rees, D. J. Thiele, *Structure* **10**, 1292 (2002).
28. G. M. Sheldrick, SHELXTL version 5 reference manual (Bruker-AXS, Madison, WI), (1994).
29. C. Brückner, S. J. Rettig, D. Dolphin, *Inorg. Chem.* **39**, 6100 (2000).
30. A. A. DiSpirito *et al.*, U.S. Provisional Patent Application Serial No. 60/434, 873 (2004).
31. C. Brükner *et al.*, *Inorg. Chem.* **39**, 6100 (2000).
32. W. Grabarse *et al.*, *J. Mol. Biol.* **303**, 329 (2000).
33. T. Selmer *et al.*, *J. Biol. Chem.* **275**, 3755 (2000).
34. O. Knosp *et al.*, *J. Bacteriol.* **159**, 341 (1984).
35. P. A. Demange *et al.*, *Biochemistry* **27**, 2745 (1988).
36. P. A. Demange *et al.*, *Biochemistry* **29**, 11041 (1990).


37. We thank J. Aube, B. Blagg, K. Camarda, D.W. Choi, T. Ebihara, A. Hooper, B. Elmore, E. Schönbrunn, and T. Williams for assistance on the project. The work was supported by NSF grant no. BES-9407286 (D.W.G.), Department of Energy grant no. 029ER2037 (A.A.D.), and University of Kansas Research Development Funds (D.W.G., C.K.L., M.A.A.). All crystallography was performed at the University of Kansas Crystallography Facility, with the diffractometer provided by NSF grant no. CHE-0079282. The crystal structure of methanobactin has been deposited at the Cambridge Crystallographic Data Centre and allocated the deposition number CCDC 241254. This work was done in fulfillment of dissertation requirements of H.J.K. at the University of Kansas, Department of Civil, Environmental, and Architectural Engineering.


**Supporting Online Material**

www.sciencemag.org/cgi/content/full/305/5690/1612/DC1
Materials and Methods
Figs. S1 and S2

25 March 2004; accepted 3 August 2004

# Activation of Endogenous Cdc42 Visualized in Living Cells

**Perihan Nalbant,* Louis Hodgson,* Vadim Kraynov, Alexei Toutchkine, Klaus M. Hahn†**

**Signaling proteins are tightly regulated spatially and temporally to perform multiple functions. For Cdc42 and other guanosine triphosphatases, the subcellular location of activation is a critical determinant of cell behavior. However, current approaches are limited in their ability to examine the dynamics of Cdc42 activity in living cells. We report the development of a biosensor capable of visualizing the changing activation of endogenous, unlabeled Cdc42 in living cells. With the use of a dye that reports protein interactions, the biosensor revealed localized activation in the trans-Golgi apparatus, microtubule-dependent Cdc42 activation at the cell periphery, and activation kinetics precisely coordinated with cell extension and retraction.**

Cdc42, a member of the Rho family of small guanosine triphosphatase (GTPase) proteins, regulates multiple cell functions, including motility, proliferation, apoptosis, and cell morphology (*1*–*3*). In order to fulfill these diverse roles, the timing and location of Cdc42 activation must be tightly controlled. The Cdc42 biosensor used here to examine the spatiotemporal dynamics of Cdc42 activation represents an in vivo application of a dye (I-SO) designed specifically to report protein conformational changes and protein interactions in living cells (*4*). In this biosensor, a domain from the Cdc42 effector protein WASP that binds only to activated Cdc42 was covalently labeled with the dye. The labeled domain showed a strong increase in fluorescence intensity upon binding to activated, underivatized Cdc42.

On the basis of the nuclear magnetic resonance (NMR) structure of the Cdc42-WASP

Department of Pharmacology, University of North Carolina School of Medicine, Chapel Hill, NC 27599–7365, USA.

*These authors contributed equally to this work.
†To whom correspondence should be addressed. E-mail: khahn@med.unc.edu